PERGAMON

International Journal of Solids and Structures 37 (2000) 6131–6153

INTERNATIONAL JOURNAL OF SOLIDS and STRUCTURES

www.elsevier.com/locate/ijsolstr

Coupled FSDT for piezothermoelectric hybrid rectangular plate

S. Kapuria [a,*], P.C. Dumir [b]

[a] *Engineers India Limited, ETD (Analysis), EIH-8th Floor, 1 Bhikajee Cama Place, New Delhi 110066 India*
[b] *Applied Mechanics Department, Indian Institute of Technology Delhi, New Delhi 110016, India*

Received 12 April 1999; in revised form 23 August 1999

Abstract

The first order shear deformation plate theory is presented for simply-supported, cross-ply laminated, rectangular hybrid plate without assuming a priori the distribution of electric potential and temperature across its thickness. The coupled constitutive equations for electric displacement are used in the charge equation of equilibrium to obtain its solution in terms of displacements of the plate. The Navier type solution for static thermoelectric load is used in three dimensional equilibrium equations to get transverse stress components. This theory is assessed by comparison with the three dimensional solution. The influence of the coupled effects is found to be significant for relatively thick piezoelectric layers.

Keywords: Coupled FSDT; Hybrid plate; Piezothermoelectric plate

1. Introduction

Smart plate and shell structures are currently being developed using piezoelectric layers for sensing, actuation and control. Exact three dimensional (3D) solutions have been presented for piezoelectric (see Ray et al., 1992; Dube et al., 1996) and hybrid (see Xu et al., 1995; Kapuria et al., 1997, 1999) simply supported rectangular plates under thermoelectromechanical loads. Assessment of uncoupled 2D classical lamination theory (CLT) and first order shear deformation theory (FSDT) developed by Tauchert (1992) and Jonnalagadda et al. (1994) for hybrid plates has been presented by Tang et al. (1996) for rectangular plates by comparison with 3D solution for simply supported edges. In general, the direct piezoelectric effect, the constitutive equations of electric displacement and the charge equation

* Corresponding author.
E-mail address: etda@eilhq.ernet.in (S. Kapuria).

0020-7683/00/$ - see front matter
PII: S0020-7683(99)00248-6

of equilibrium are ignored and the electric potential is assumed a priori to vary linearly across the thickness of the actuated layer. Tzou and Ye (1994) have included the direct piezoelectric effect in their theory in an adhoc manner and did not satisfy the charge equation of equilibrium. Noda and Kimura (1998) have presented classical plate theory formulation in which the charge equations of equilibrium are solved in terms of the deflection of the plate. However, the temperature is apriori assumed to vary linearly across the thickness of the hybrid plate.

In this work, a coupled first order shear deformation plate theory is presented for rectangular hybrid plate without any a priori assumption of the distribution of electric potential and temperature across its thickness. The thermal equilibrium equations are solved exactly. The coupled constitutive equations of electric displacement are used in the charge equations of equilibrium to obtain the exact solution for the electric potential in terms of the displacements of the panel. Fourier series solution is presented for simply-supported hybrid plates consisting of cross-ply composite elastic substrate with some piezoelectric layers subjected to static electrothermomechanical load. This solution is used in 3D equilibrium equations to obtain transverse stresses. The deflection and stresses obtained by the present theory are compared with the 3D solution to assess this theory. The coupled effects have significant influence on the response for relatively thick piezoelectric layers.

2. Solution for coupled FSDT

Consider an L-layered hybrid rectangular plate of sides a and b, made of cross-ply composite laminate and piezoelectric laminae with the principal directions along the Cartesian coordinates. The Cartesian coordinates x, y span the midplane. At $x = 0, a$, and at $y = 0, b$ the panel is simply-supported, electrically grounded and held at the stress-free reference temperature. The electric field induced due to stress and temperature is not neglected compared to the electric field applied for actuation. Denoting differentiation by subscript comma, in FSDT the displacements (u, v, w) at (x, y, z) are approximated as

$$u = u^0(x, y) + z\psi_x(x, y), \quad v = v^0(x, y) + z\psi_y(x, y), \quad w = w^0(x, y), \tag{1}$$

where u^0, v^0, w^0 are displacements of midplane and ψ_x, ψ_y are rotations of its normal. The strains are

$$\begin{bmatrix} \varepsilon_x \\ \varepsilon_y \\ \gamma_{xy} \end{bmatrix} = \varepsilon^0 + z\kappa, \quad \varepsilon^0 = \begin{bmatrix} u^0_{,x} \\ v^0_{,y} \\ u^0_{,y} + v^0_{,x} \end{bmatrix}, \quad \kappa = \begin{bmatrix} \psi_{x,\,x} \\ \psi_{y,\,y} \\ \psi_{x,\,y} + \psi_{y,\,x} \end{bmatrix}, \quad \begin{bmatrix} \varepsilon_z \\ \gamma_{yz} \\ \gamma_{zx} \end{bmatrix} = \begin{bmatrix} 0 \\ \psi_y + w^0_{,y} \\ \psi_x + w^0_{,x} \end{bmatrix} \tag{2}$$

For linear orthorohmbic piezoelectric material of class mm2, polarised in direction z with principal directions along x, y, z, the constitutive equations relating the stress σ, the strain ε, the electric field $E = (E_x, E_y, E_z)^{\mathrm{T}}$, the electric displacement $D = (D_x, D_y, D_z)^{\mathrm{T}}$ and the temperature rise T above the stress-free reference temperature, are related by

$$\varepsilon = S\sigma + d^{\mathrm{T}}E + \alpha T, \qquad D = e\varepsilon + \eta E + pT \tag{3}$$

with $e = dS^{-1}$ and superscript T denotes matrix transpose. S, d, e, α, η, p are respectively the matrices of elastic compliance, piezoelectric strain constants, piezoelectric stress constants, coefficients of thermal expansion, permittivities for constant strain field and pyroelectric constants for constant strain field, with

$$S=\begin{bmatrix} 1/E_1 & -\nu_{21}/E_2 & -\nu_{31}/E_3 & 0 & 0 & 0 \\ -\nu_{12}/E_1 & 1/E_2 & -\nu_{32}/E_3 & 0 & 0 & 0 \\ -\nu_{13}/E_1 & -\nu_{23}/E_2 & 1/E_3 & 0 & 0 & 0 \\ 0 & 0 & 0 & 1/G_{23} & 0 & 0 \\ 0 & 0 & 0 & 0 & 1/G_{31} & 0 \\ 0 & 0 & 0 & 0 & 0 & 1/G_{12} \end{bmatrix}, \quad d^{\mathrm{T}}=\begin{bmatrix} 0 & 0 & d_{31} \\ 0 & 0 & d_{32} \\ 0 & 0 & d_{33} \\ 0 & d_{24} & 0 \\ d_{15} & 0 & 0 \\ 0 & 0 & 0 \end{bmatrix},$$

$$\alpha=\begin{bmatrix} \alpha_1 \\ \alpha_2 \\ \alpha_3 \\ 0 \\ 0 \\ 0 \end{bmatrix} \eta=\begin{bmatrix} \eta_{11} & 0 & 0 \\ 0 & \eta_{22} & 0 \\ 0 & 0 & \eta_{33} \end{bmatrix}, \quad e=\begin{bmatrix} 0 & 0 & 0 & 0 & e_{15} & 0 \\ 0 & 0 & 0 & e_{24} & 0 & 0 \\ e_{31} & e_{32} & e_{33} & 0 & 0 & 0 \end{bmatrix}, \quad p=\begin{bmatrix} 0 \\ 0 \\ p_3 \end{bmatrix}, \tag{4}$$

$$E=-\begin{bmatrix} \phi_{,x} \\ \phi_{,y} \\ \phi_{,z} \end{bmatrix},$$

where E_i are Young's moduli, ν_{ij} are Poisson's ratios, G_{ij} are shear moduli and ϕ is the electric potential. As by Tauchert (1992), Jonnalagadda et al. (1994) and Tang et al. (1996), the temperature dependence of material properties has not been included. Using Eq. (2) and the plate theory assumption of $\sigma_z \simeq 0$, Eq. (3) yields

$$\begin{bmatrix} \sigma_x \\ \sigma_y \\ \tau_{xy} \end{bmatrix}=\begin{bmatrix} Q_{11} & Q_{12} & 0 \\ Q_{21} & Q_{22} & 0 \\ 0 & 0 & Q_{66} \end{bmatrix}\begin{bmatrix} \varepsilon_x \\ \varepsilon_y \\ \gamma_{xy} \end{bmatrix}+\begin{bmatrix} e_{31} \\ e_{32} \\ 0 \end{bmatrix}\phi_{,z}-\begin{bmatrix} \beta_1 \\ \beta_2 \\ 0 \end{bmatrix}T, \quad \begin{bmatrix} \tau_{yz} \\ \tau_{zx} \end{bmatrix}=\begin{bmatrix} Q_{44}\gamma_{yz}+e_{24}\phi_{,y} \\ Q_{55}\gamma_{zx}+e_{15}\phi_{,x} \end{bmatrix}; \tag{5}$$

$$D_x=e_{15}\gamma_{zx}-\eta_{11}\phi_{,x}, \quad D_y=e_{24}\gamma_{yz}-\eta_{22}\phi_{,y}, \quad D_z=e_{31}\varepsilon_x+e_{32}\varepsilon_y-\eta_{33}\phi_{,z}+p_3T, \tag{6}$$

with

$$\begin{aligned} &Q_{11}=\frac{E_1}{1-\nu_{12}\nu_{21}}, \quad Q_{12}=\frac{\nu_{12}E_2}{1-\nu_{12}\nu_{21}}, \quad Q_{22}=\frac{E_2}{1-\nu_{12}\nu_{21}}, \quad Q_{66}=G_{12}, e_{31}=Q_{11}d_{31}+Q_{12}d_{32}, \\ &e_{32}=Q_{12}d_{31}+Q_{22}d_{32}, \quad \beta_1=Q_{11}\alpha_1+Q_{12}\alpha_2, \quad \beta_2=Q_{12}\alpha_1+Q_{22}\alpha_2, Q_{44}=G_{23}, \quad Q_{55}=G_{31}, \\ &e_{24}=Q_{44}d_{24}, \quad e_{15}=Q_{55}d_{15} \end{aligned} \tag{7}$$

The force and moment resultants (N_x, N_y, N_{xy}, Q_x, Q_y, M_x, M_y, M_{xy}) for the edge of the midplane and the load (p_x, p_y, p_z, m_x, m_y) per unit area of the midplane are defined in terms of the stresses by

$$\left[N_x, N_y, N_{xy}, Q_x, Q_y, M_x, M_y, M_{xy}\right]=\int_{-h/2}^{h/2}[\sigma_x, \sigma_y, \tau_{xy}, \tau_{zx}, \tau_{zy}, z\sigma_x, z\sigma_y, z\tau_{xy}]\,\mathrm{d}z,$$

$$(p_x, p_y, p_z, m_x, m_y)=[\tau_{zx}, \tau_{zy}, \sigma_z, z\tau_{zx}, z\tau_{zy}]\Big|_{-h/2}^{h/2} \tag{8}$$

where h is the plate thickness. Using expressions of stresses from Eq. (5) in Eq. (8) yields following relations between the resultants and displacements:

$$\begin{bmatrix} N \\ M \end{bmatrix} = \begin{bmatrix} A & B \\ B & D \end{bmatrix} \begin{bmatrix} \varepsilon^0 \\ \kappa \end{bmatrix} + \begin{bmatrix} N^e \\ M^e \end{bmatrix} + \begin{bmatrix} N^t \\ M^t \end{bmatrix}, \quad \begin{bmatrix} Q_x \\ Q_y \end{bmatrix} = \begin{bmatrix} A_{55}\left(w^0_{,x} + \psi_x\right) + Q^e_x \\ A_{44}\left(w^0_{,y} + \psi_y\right) + Q^e_y \end{bmatrix} \tag{9}$$

and

$$\begin{bmatrix} N^e_x, N^e_y, N^t_x, N^t_y \\ M^e_x, M^e_y, M^t_x, M^t_y \end{bmatrix} = \int_{-h/2}^{h/2} \begin{bmatrix} 1 \\ z \end{bmatrix} \left[e_{31}\phi_{,z}, e_{32}\phi_{,z}, -\beta_1 T, -\beta_2 T\right] \mathrm{d}z,$$
$$\begin{bmatrix} Q^e_x \\ Q^e_y \end{bmatrix} = \int_{-h/2}^{h/2} \begin{bmatrix} e_{15}\phi_{,x} \\ e_{24}\phi_{,y} \end{bmatrix} \mathrm{d}z \tag{10}$$

$[A_{ij}, B_{ij}, D_{ij}] = \int_{-h/2}^{h/2} k^2_{ij} Q_{ij}[1, z, z^2]\,\mathrm{d}z$ and $k_{ij} = 1$ except for $k^2_{44} = k^2_{55} = 5/6$. The boundary conditions are taken as:

$$x = 0, a: \quad N_x = 0, \quad v^0 = w^0 = 0, \quad \psi_y = 0, \quad M_x = 0, \quad T = 0, \quad \phi = 0,$$

$$y = 0, b: \quad N_y = 0, \quad u^0 = w^0 = 0, \quad \psi_x = 0, \quad M_y = 0, \quad T = 0, \quad \phi = 0 \tag{11}$$

Let the interfaces of the actuator layers with the elastic substrate be grounded, the ambient temperatures at $z = \mp h/2$ be $T_1(x)$, $T_2(x)$ and h_1, h_2 be the convective heat transfer coefficients at $z = \mp h/2$. The thermal and the electric potential problems are solved exactly. The variables are expanded in Fourier series as:

$$\left(u^0, \psi_x, Q_x, p_x, m_x, \tau_{zx}\right) = \sum_{m=1}^{\infty}\sum_{n=1}^{\infty} \left(u^0, \psi_x, Q_x, p_x, m_x, \tau_{zx}\right)_{mn} \cos\bar{m}x \sin\bar{n}y,$$

$$\left(v^0, \psi_y, Q_y, p_y, m_y, \tau_{yz}\right) = \sum_{m=1}^{\infty}\sum_{n=1}^{\infty} \left(v^0, \psi_y, Q_y, p_y, m_y, \tau_{yz}\right)_{mn} \sin\bar{m}x \cos\bar{n}y,$$

$$\left(w^0, p_z, \sigma_x, \sigma_y, \sigma_z, N_x, N_y, M_x, M_y, T, \phi\right)$$
$$= \sum_{m=1}^{\infty}\sum_{n=1}^{\infty} \left(w^0, p_z, \sigma_x, \sigma_y, \sigma_z, N_x, N_y, M_x, M_y, T, \phi\right)_{mn} \sin\bar{m}x \sin\bar{n}y,$$

$$\left(\tau_{xy}, N_{xy}, M_{xy}\right) = \sum_{m=1}^{\infty}\sum_{n=1}^{\infty} \left(\sigma_{xy}, N_{xy}, M_{xy}\right)_{mn} \cos\bar{m}x \cos\bar{n}y, \tag{12}$$

with $\bar{m} = m\pi/a$, $\bar{n} = n\pi/b$. The thermal equilibrium equation without body heat source is

$$k_x T_{,xx} + k_y T_{,yy} + k_z T_{,zz} = 0, \quad \text{i.e., } T_{mn,\,zz} - \left(\bar{m}^2 k_x + \bar{n}^2 k_y\right) T_{mn}/k_z = 0, \tag{13}$$

where k_x, k_y, k_z are thermal conductivity coefficients. The solution for the kth layer between z_{k-1} and z_k in terms of constants A^{mn}_{ik} is

$$T^{(k)}_{mn}(z) = \sum_{i=1}^{2} A^{mn}_{ik}\, \mathrm{e}^{z\rho_{ik}} \tag{14}$$

where $\rho_{1k} = -\rho_{2k} = \mu^{(k)}_{mn} = [(\bar{m}^2 k^{(k)}_x + \bar{n}^2 k^{(k)}_y)/k^{(k)}_z]^{1/2}$. The superscript k refers to the kth lamina. This superscript will often be omitted for simplicity. Let the (m, n)th Fourier component of the heat flow rate and temperature at the surface at z_k be $q^k_{mn} = -k^{(k)}_z T^{(k)}_{mn,\,z}|_{z=z_k}$ and T^k_{mn}. Using Eq. (14), the transfer function H_k for these is obtained as

$$\begin{bmatrix} T^k_{mn} \\ q^k_{mn} \end{bmatrix} = H_k \begin{bmatrix} T^{(k-1)}_{mn} \\ q^{(k-1)}_{mn} \end{bmatrix}, \quad H_k = \begin{bmatrix} \cosh\bar{\mu}^{(k)}_{mn} & -\sinh\bar{\mu}^{(k)}_{mn}/c \\ -c\sinh\bar{\mu}^{(k)}_{mn} & \cosh\bar{\mu}^{(k)}_{mn} \end{bmatrix},$$
$$\begin{bmatrix} \mathrm{e}^{\mu^*} & A^{mn}_{1k} \\ \mathrm{e}^{-\mu^*} & A^{mn}_{2k} \end{bmatrix} = \begin{bmatrix} 0.5 & -0.5/c \\ 0.5 & 0.5/c \end{bmatrix} \begin{bmatrix} T^{(k-1)}_{mn} \\ q^{(k-1)}_{mn} \end{bmatrix} \tag{15}$$

with $c = k^{(k)}_z \mu^{(k)}_{mn}$, $\bar{\mu}^{(k)}_{mn} = \mu^{(k)}_{mn}(z_k - z_{k-1})$, $\mu^* = \mu^{(k)}_{mn} z_{k-1}$. The global transfer function H is obtained as

$$\begin{bmatrix} T^L_{mn} \\ q^L_{mn} \end{bmatrix} = H \begin{bmatrix} T^0_{mn} \\ q^0_{mn} \end{bmatrix}, \quad \text{where} \quad H = \begin{bmatrix} H_{11} & H_{12} \\ H_{21} & H_{22} \end{bmatrix} = H_L H_{L-1} \cdots H_2 H_1. \tag{16}$$

The thermal boundary conditions at $z = \mp h/2$ are:

$$z = \frac{-h}{2}: \quad q^0_{mn} = -h_1\left(T^0_{mn} - T_{1_{mn}}\right), \quad z = \frac{h}{2}: \quad q^L_{mn} = h_2\left(T^L_{mn} - T_{2_{mn}}\right) \tag{17}$$

The case of prescribed surface temperatures corresponds to $h_1 = h_2 = \infty$. Using Eqs. (16) and (17), yields

$$T^0_{mn} = \frac{(h_2 H_{12} - H_{22}) h_1 T_{1_{mn}} - h_2 T_{2_{mn}}}{H_{21} - h_2 H_{11} - h_1 H_{22} + h_1 h_2 H_{12}}, \qquad q^0_{mn} = -h_1\left(T^0_{mn} - T_{1_{mn}}\right) \tag{18}$$

The constants A^{mn}_{ik} in the solution (14) for T_{mn} are then obtained successively using Eq. (15).

Using the constitutive Eq. (6), the expansions (12) and the solution (14) for temperature, in the charge equation of equilibrium without any body charge, viz., $D_{x,\,x} + D_{y,\,y} + D_{z,\,z} = 0$, reduces it to the following form for a point in the kth layer:

$$\eta_{33}\phi_{mn,\,zz} - \left(\bar{m}^2\eta_{11} + \bar{n}^2\eta_{22}\right)\phi_{mn}$$
$$= -\bar{m}(e_{31} + e_{15})\psi_{x_{mn}} - \bar{n}(e_{32} + e_{24})\psi_{y_{mn}} - \left(\bar{m}^2 e_{15} + \bar{n}^2 e_{24}\right) w^0_{mn} + p_3 \sum_{i=1}^{2} \rho_{ik} A^{mn}_{ik}\, \mathrm{e}^{z\rho_{ik}} \tag{19}$$

Its solution in terms of constants B^{mn}_{ik} is given by

$$\phi_{mn} = \sum_{i=1}^{2} B^{mn}_{ik}\, \mathrm{e}^{\gamma_{ik} z} + \frac{\bar{m}(e_{31} + e_{15})^{(k)}\psi_{x_{mn}} + \bar{n}(e_{32} + e_{24})^{(k)}\psi_{y_{mn}} + \left(\bar{m}^2 e^{(k)}_{15} + \bar{n}^2\, \mathrm{e}^{(k)}_{24}\right) w^0_{mn}}{\left(\alpha^2_{mn}\eta_{33}\right)^{(k)}}$$
$$+ \left(\frac{p_3}{\eta_{33}}\right)^{(k)} \sum_{i=1}^{2} \frac{\rho_{ik} A^{mn}_{ik}\, \mathrm{e}^{\rho_{ik} z}}{\left(\rho^2_{ik} - \alpha^2_{mn}\right)^{(k)}} \tag{20}$$

where $\alpha_{mn}^{(k)}=[(\eta_{11}^{(k)}\bar{m}^2+\eta_{22}^{(k)}\bar{n}^2)/\eta_{33}^{(k)}]^{1/2}$, $\gamma_{1k}=-\gamma_{2k}=\alpha_{mn}^{(k)}$. Using Eq. (20) in (6) yields

$$D_{z_{mn}} = -\left[\bar{m}e_{31}^{(k)}\left(u_{mn}^0 + z\psi_{x_{mn}}\right)\right] - \left[\bar{n}e_{32}^{(k)}\left(v_{mn}^0 + z\psi_{y_{mn}}\right)\right] - \eta_{33}^{(k)}\sum_{i=1}^{2} B_{ik}^{mn}\gamma_{ik}\,\mathrm{e}^{\gamma_{ik}z}$$
$$- p_3^{(k)}\sum_{i=1}^{2}\frac{A_{ik}^{mn}\alpha_{mn}^{(k)^2}\,\mathrm{e}^{\rho_{ik}z}}{\rho_{ik}^2-\alpha_{mn}^{(k)^2}} \tag{21}$$

Substituting T and ϕ from Eqs. (14) and (20) in Eq. (10) yields

$$\begin{bmatrix} N_x^t & M_x^t \\ N_y^t & M_y^t \end{bmatrix}_{mn} = -\sum_{k=1}^{L}\sum_{i=1}^{2}\begin{bmatrix}\beta_1\\ \beta_2\end{bmatrix}^{(k)}\begin{bmatrix}\bar{\rho}_{ik} & \tilde{\rho}_{ik}\end{bmatrix}A_{ik}^{mn}/\rho_{ik},$$

$$\begin{bmatrix} N_x^e & M_x^e \\ N_y^e & M_y^e \end{bmatrix}_{mn} = \sum_{k=1}^{L}\sum_{i=1}^{2}\begin{bmatrix}e_{31}\\ e_{32}\end{bmatrix}^{(k)}\begin{bmatrix}\bar{\gamma}_{ik}\tilde{\gamma}_{ik}\end{bmatrix}B_{ik}^{mn} + \begin{bmatrix} \bar{N}_1^e & \bar{M}_1^e \\ \bar{N}_2^e & \bar{M}_2^e \end{bmatrix}_{mn},$$

$$\begin{bmatrix} Q_x^e \\ Q_y^e \end{bmatrix}_{mn} = \sum_{k=1}^{L}\sum_{i=1}^{2}\begin{bmatrix}\bar{m}e_{15}\\ \bar{n}e_{24}\end{bmatrix}\frac{\bar{\gamma}_{ik}}{\gamma_{ik}}B_{ik}^{mn} + \begin{bmatrix} Q_1^{et} \\ Q_2^{et} \end{bmatrix}_{mn} + \begin{bmatrix} Q_1^0 \\ Q_2^0 \end{bmatrix}_{mn} w_{mn}^0 + \begin{bmatrix} Q_1^1 \\ Q_2^1 \end{bmatrix}_{mn}\psi_{x_{mn}} + \begin{bmatrix} Q_1^2 \\ Q_2^2 \end{bmatrix}_{mn}\psi_{y_{mn}} \tag{22}$$

where

$$\bar{g}_{ik} = \mathrm{e}^{g_{ik}z_k} - \mathrm{e}^{g_{ik}z_{k-1}}, \quad \tilde{g}_{ik} = z_k\,\mathrm{e}^{g_{ik}z_k} - z_{k-1}\,\mathrm{e}^{g_{ik}z_{k-1}} - \bar{g}_{ik}/g_{ik}, \quad \text{for } g_{ij}=\gamma_{ij},\rho_{ij},$$

$$\begin{bmatrix} \bar{N}_j^e \\ \bar{M}_j^e \end{bmatrix}_{mn} = \sum_{k=1}^{L}\sum_{i=1}^{2}\frac{p_3^{(k)}\rho_{ik}e_{3j}^{(k)}}{\eta_{33}^{(k)}\left(\rho_{ik}^2-\alpha_{mn}^{(k)^2}\right)}A_{ik}^{mn}\begin{bmatrix}\bar{\rho}_{ik}\\ \tilde{\rho}_{ik}\end{bmatrix}, \quad j=1,2;$$

$$\begin{bmatrix} Q_1^{et} \\ Q_2^{et} \end{bmatrix}_{mn} = \sum_{k=1}^{L}\begin{bmatrix}\bar{m}e_{15}^{(k)}\\ \bar{n}e_{24}^{(k)}\end{bmatrix}\sum_{i=1}^{2}\frac{p_3^{(k)}\bar{\rho}_{ik}A_{ik}^{mn}}{\eta_{33}^{(k)}\left(\rho_{ik}^2-\alpha_{mn}^{(k)^2}\right)}.$$

$$\begin{bmatrix} Q_1^p \\ Q_2^p \end{bmatrix}_{mn} = \sum_{k=1}^{L}\begin{bmatrix}\bar{m}e_{15}^{(k)}\\ \bar{n}e_{24}^{(k)}\end{bmatrix}\frac{(z_k-z_{k-1})l_pk}{\eta_{33}^{(k)}\alpha_{mn}^{(k)^2}}, \quad p=0,1,2: \tag{23}$$

with

$$l_{0k} = \bar{m}^2e_{15}^{(k)} + \bar{n}^2e_{24}^{(k)}, \quad l_{1k} = \bar{m}(e_{31}+e_{15})^{(k)}, \quad l_{2k} = \bar{n}(e_{32}+e_{24})^{(k)}$$

The equations of equilibrium without body force are:

$$N_{x,\,x} + N_{xy,\,y} + p_x = 0, \quad N_{xy,\,x} + N_{y,\,y} + p_y = 0, \quad Q_{x,\,x} + Q_{y,\,y} + p_z = 0, \tag{24a}$$

$$M_{x,\,x} + M_{xy,\,y} - Q_x + m_x = 0, \quad M_{xy,\,x} + M_{y,\,y} - Q_y + m_y = 0. \tag{24b}$$

Using Eqs. (9), (2) and (22), these reduce to following algebraic equations:

$$X^{mn}U^{mn} = \bar{P}^{mn} + \bar{E}^{mn}B^{mn} - R^{mn}U^{mn} \tag{25}$$

with

$$U^{mn} = \begin{bmatrix} u^0 & v^0 & w^0 & \psi_x & \psi_y \end{bmatrix}^{\mathrm{T}}_{mn}, \quad \bar{P}_1^{mn} = \left[p_x + \bar{m}\left(\bar{N}_1^e + N_x^t\right)\right]_{mn}, \quad \bar{P}_2^{mn} = \left[p_y + \bar{n}\left(\bar{N}_2^e + N_y^t\right)\right]_{mn},$$

$$\bar{P}_3^{mn} = \left[p_z - \bar{m}Q_1^{et} - \bar{n}Q_2^{et})\right]mn, \quad \bar{P}_4^{mn} = \left[m_x + \bar{m}\left(\bar{M}_1^e + M_x^t\right) - Q_1^{et}\right]_{mn},$$

$$\bar{P}_5^{mn} = \left[m_y + \bar{n}\left(\bar{M}_2^e + M_y^t\right) - Q_2^{et}\right]mn,$$

$$\bar{E}^{mn}_{1,\,2k-2+i} = \bar{m}e_{31}^{(k)}\bar{\gamma}_{ik}, \quad \bar{E}^{mn}_{2,\,2k-2+i} = \bar{n}e_{32}^{(k)}\bar{\gamma}_{ik}, \quad i = 1, 2,\ k = 1, \ldots, L$$

$$\bar{E}^{mn}_{3,\,2k-2+i} = -\left(\bar{m}^2 e_{15}^{(k)} + \bar{n}^2 e_{24}^{(k)}\right)\bar{\gamma}_{ik}/\gamma_{ik}, \quad \bar{E}^{mn}_{4,\,2k-2+i} = \bar{m}\left(e_{31}^{(k)}\tilde{\gamma}_{ik} - e_{15}^{(k)}\bar{\gamma}_{ik}/\gamma_{ik}\right),$$

$$\bar{E}^{mn}_{5,\,2k-2+i} = \bar{n}\left(e_{32}^{(k)}\tilde{\gamma}_{ik} - e_{24}^{(k)}\bar{\gamma}_{ik}/\gamma_{ik}\right), \quad R_{ij}^{mn} = R_{ji}^{mn} = 0,\ i = 1, 2;\ j = 1, \ldots, 5,$$

$$R_{33}^{mn} = \left(\bar{m}Q_1^0 + \bar{n}Q_2^0\right)_{mn}, \quad R_{34}^{mn} = \left(\bar{m}Q_1^1 + \bar{n}Q_2^1\right)_{mn}, \quad R_{35}^{mn} = \left(\bar{m}Q_1^2 + \bar{n}Q_2^2\right)_{mn},$$

$$R_{43}^{mn} = Q^0_{1_{mn}}, \quad R_{44}^{mn} = Q^1_{1_{mn}}, \quad R_{45}^{mn} = Q^2_{1_{mn}}, \quad R_{53}^{mn} = Q^0_{2_{mn}}, \quad R_{54}^{mn} = Q^1_{2_{mn}}, \quad R_{55}^{mn} = Q^2_{2_{mn}},$$

$$X_{11}^{mn} = \bar{m}^2 A_{11} + \bar{n}^2 A_{66}, \quad X_{12}^{mn} = \bar{m}\bar{n}(A_{12} + A_{66}), \quad X_{13}^{mn} = X_{23}^{mn} = 0,$$

$$X_{14}^{mn} = \bar{m}^2 B_{11} + \bar{n}^2 B_{12}, X_{15}^{mn} = X_{24}^{mn} = \bar{m}\bar{n}(B_{12} + B_{66}), \quad X_{22} = \bar{m}^2 A_{66} + \bar{n}^2 A_{22},$$

$$X_{25} = \bar{m}^2 B_{66} + \bar{n}^2 B_{22},$$

$$X_{33} = \bar{m}^2 A_{55} + \bar{n}^2 A_{44}, \quad X_{34} = \bar{m}A_{55}, \quad X_{35} = \bar{n}A_{44},$$

$$X_{44} = \bar{m}^2 D_{11} + \bar{n}^2 D_{66} + A_{55}, \quad X_{45} = \bar{m}\bar{n}(D_{12} + D_{66}), \quad X_{55} = \bar{m}^2 D_{66} + \bar{n}^2 D_{22} + A_{44}, \quad X_{ij}^{mn} = X_{ji}^{mn},$$

$$B^{mn} = \begin{bmatrix} B_{11}^{mn} & B_{21}^{mn} & B_{12}^{mn} & B_{22}^{mn} \cdots B_{1L}^{mn} & B_{2L}^{mn} \end{bmatrix}^{\mathrm{T}}.$$

The electric boundary conditions at $z = \pm h/2$ may be prescribed values of ϕ or D_z. The electric potential of some interfaces may be prescribed. At an interface where the potential is not prescribed, the two conditions of continuity of ϕ and D_z are to be satisfied. At an interface where the potential is prescribed, the conditions are that the potential of the two layers at this interface must equal the prescribed potential. Thus the $2L$ unknown coefficients B_{ij}^{mn} can be solved in terms of the displacement variables. In particular, the following electrical boundary conditions are considered:

$$z = -h/2: \quad \phi = \phi_1(x, y), \quad z = h/2: \quad \phi = \phi_2(x, y) \text{ or } D_z = D_2(x, y), \tag{26a}$$

$$\text{optionally at } z = z_1: \quad \phi = \phi_3(x, y). \tag{26b}$$

The continuity conditions at the interfaces are:

$$\left[(\phi, D_z)|_{z=z_k}\right]^{(k)} = \left[(\phi, D_z)|_{z=z_k}\right]^{(k+1)}, \quad k = 1, \ldots, L-1 \tag{26c}$$

In case ϕ_3 is applied, the continuity condition for D_z at the first interface ($k = 1$) is replaced by Eq. (26b). Substitution of Eqs. (20) and (21) into conditions Eq. (26) yields following algebraic equations for B_{ij}^{mn} in terms of the displacement variables:

$$Y^{mn} B^{mn} = F^{mn} U^{mn} + G^{mn} \tag{27}$$

The non-zero elements of Y^{mn}, F^{mn}, G^{mn} are:

$$Y^{mn}_{1j} = \mathrm{e}^{\gamma_{j1} z_0}, \quad Y^{mn}_{2k,\,2k-2+j} = \mathrm{e}^{\gamma_{jk} z_k}, \quad Y^{mn}_{2k,\,2k+j} = -\mathrm{e}^{\gamma_{j,\,k+1} z_k},$$

$$Y^{mn}_{2k+1,\,2k-2+j} = \eta_{33}^{(k)} \gamma_{jk}\, \mathrm{e}^{\gamma_{j,\,k} z_k}, \quad Y^{mn}_{2k+1,\,2k+j} = -\eta_{33}^{(k+1)} \gamma_{j,\,k+1}\, \mathrm{e}^{\gamma_{j,\,k+1} z_k}, \quad \text{for } j = 1, 2;\ k = 1, \ldots, L-1$$

if ϕ_2 is prescribed, then

$$Y^{mn}_{2L,\,2L-2+j} = \mathrm{e}^{\gamma_{jL} z_L},$$

else

$$Y^{mn}_{2L,\,2L-2+j} = \eta_{33}^{(L)} \gamma_{jL}\, \mathrm{e}^{\gamma_{jL} z_L},$$

if ϕ_3 is prescribed:

$$Y^{mn}_{3j} = \mathrm{e}^{\gamma_{j1} z_1},$$

$$F^{mn}_{13} = c_3^{(1)}, \quad F^{mn}_{14} = c_4^{(1)}, \quad F^{mn}_{15} = c_5^{(1)}, \quad G^{mn}_{1} = c_t^{(1)} + \phi_{1_{mn}},$$

$$F^{mn}_{2k,\,3} = c_3^{(k)} - c_3^{(k+1)}, \quad F^{mn}_{2k,\,4} = c_4^{(k)} - c_4^{(k+1)}, \quad F^{mn}_{2k,\,5} = c_5^{(k)} - c_5^{(k+1)}, \quad G^{mn}_{2k} = c_t^{(k)} - c_t^{(k+1)},$$

$$F^{mn}_{2k+1,\,1} = \bar{c}_1^{(k)} - \bar{c}_1^{(k+1)}, \quad F^{mn}_{2k+1,\,2} = \bar{c}_2^{(k)} - \bar{c}_2^{(k+1)}, \quad F^{mn}_{2k+1,\,4} = \bar{c}_4^{(k)} - \bar{c}_4^{(k+1)},$$

$$F^{mn}_{2k+1,\,5} = \bar{c}_5^{(k)} - \bar{c}_5^{(k+1)}, \quad G^{mn}_{2k+1} = \bar{c}_t^{(k)} - \bar{c}_t^{(k+1)}, \quad \text{for } k = 1, \ldots, L-1$$

if ϕ_2 is prescribed:

$$F^{mn}_{2L,\,3} = c_3^{(L)}, \quad F^{mn}_{2L,\,4} = c_4^{(L)}, \quad F^{mn}_{2L,\,5} = c_5^{(L)}, \quad G^{mn}_{2L} = c_t^{(L)} + \phi_{2_{mn}},$$

if D_2 is prescribed:

$$F^{mn}_{2L,\,1} = \bar{c}_1^{(L)}, \quad F^{mn}_{2L,\,2} = \bar{c}_2^{(L)}, \quad F^{mn}_{2L,\,4} = \bar{c}_4^{(L)}, \quad F^{mn}_{2L,\,5} = \bar{c}_5^{(L)}, \quad G^{mn}_{2L} = \bar{c}_t^{(L)} + D_{2_{mn}},$$

if ϕ_3 is prescribed:

$$F_{33}^{mn} = c_3^{(1)}, \quad F_{34}^{mn} = c_4^{(1)}, \quad F_{35}^{mn} = c_5^{(1)}, \quad G_3^{mn} = c_t^{(1)} + \phi_{3_{mn}},$$

where

$$c_3^{(k)} = -\left(\frac{\bar{m}^2 e_{15} + \bar{n}^2 e_{24}}{\alpha_{mn}^2 \eta_{33}}\right)^{(k)}, \quad c_4^{(k)} = -\bar{m}\left(\frac{e_{31} + e_{15}}{\alpha_{mn}^2 \eta_{33}}\right)^{(k)},$$

$$c_5^{(k)} = -\bar{n}\left(\frac{e_{32} + e_{24}}{\alpha_{mn}^2 \eta_{33}}\right)^{(k)}, \quad c_t^{(k)} = -\left(\frac{p_3}{\eta_{33}} \sum_{i=1}^{2} \frac{A_{ik}^{mn} \rho_{ik} e^{\rho_{ik} z_k}}{\rho_{ik}^2 - \alpha_{mn}^2}\right)^{(k)},$$

$$\bar{c}_1^{(k)} = -\bar{m} e_{31}^{(k)}, \quad \bar{c}_2^{(k)} = -\bar{n} e_{32}^{(k)}, \quad \bar{c}_4^{(k)} = -\bar{m} z_k e_{31}^{(k)}, \quad \bar{c}_5^{(k)} = -\bar{n} z_k e_{32}^{(k)},$$

$$\bar{c}_t^{(k)} = -\left(p_3 \sum_{i=1}^{2} \frac{A_{ik}^{mn} \alpha_{mn}^2 e^{\rho_{ik} z_k}}{\rho_{ik}^2 - \alpha_{mn}^2}\right)^{(k)}.$$

The solution of Eq. (27) yields

$$B^{mn} = \bar{F}^{mn} U^{mn} + \bar{G}^{mn} \tag{28}$$

where $\bar{F}^{mn} = [Y^{mn}]^{-1} F^{mn}$, $\bar{G}^{mn} = [Y^{mn}]^{-1} G^{mn}$. Substituting B^{mn} from Eq. (28) in Eq. (25) yields following explicit algebraic equations for U^{mn}:

$$\left(X^{mn} - \bar{E}^{mn} \bar{F}^{mn} + R^{mn}\right) U^{mn} = \bar{P}^{mn} + \bar{E}^{mn} \bar{G}^{mn} \tag{29}$$

These are solved for U^{mn} and B^{mn} are then obtained from Eq. (28). A convergence study would decide the number of terms to be retained in the Fourier series for desired accuracy. The inplane stresses are obtained from Eq. (5) using Eqs. (12), (14) and (20). Three-dimensional equilibrium equations are then used to obtain transverse stresses: $\tau_{zx} = -\int(\sigma_{x,\,x} + \tau_{xy,\,y})\,\mathrm{d}z$, $\tau_{zy} = -\int(\sigma_{y,\,y} + \tau_{xy,\,x})\,\mathrm{d}z$, $\sigma_z = -\int(\tau_{zx,\,x} + \tau_{zy,\,y})\,\mathrm{d}z$.

3. Solution for coupled CLT

The transverse shear strains are neglected in CLT. The solution for coupled CLT is similar to that for the coupled FSDT with the following changes. The shear stress resultants Q_x, Q_y are not obtained from the constitutive equations (5), but from the equilibrium equations (24b). These are substituted in the third equilibrium equation of (24a) to yield

$$M_{x,\,xx} + 2M_{xy,\,xy} + M_{y,\,yy} + m_{x,\,x} + m_{y,\,y} + p_z = 0. \tag{30}$$

The fourth and fifth equilibrium equations (24b) are replaced by the following equations for zero transverse shear strains:

$$\psi_x = -w_x^0, \qquad \psi_y = -w_y^0. \tag{31}$$

Table 1
Comparative study of 2D solutions for thermal load ($h_a/h = 0.1$)

	S	Exact	Uncoupled		Coupled (no pyroelectric effect)		Coupled	
			FSDT	CLT	FSDT	CLT	FSDT	CLT
$\bar{w}$ (0.5a, 0.5b, 0)	4	−0.3418	−0.5832	−0.5718	−0.5811	−0.5705	−0.5697	−0.5565
	10	−0.5372	−0.5866	−0.5840	−0.5879	−0.5855	−0.5697	−0.5668
	100	−0.5696	−0.5864	−0.5864	−0.5886	−0.5886	−0.5688	−0.5688
$\bar{u}$ (0, 0.5b, −0.5h)	4	−2.238	−1.553	−1.672	−1.551	−1.671	−1.541	−1.659
	10	−1.873	−1.758	−1.785	−1.759	−1.786	−1.743	−1.769
	100	−1.796	−1.809	−1.809	−1.811	−1.811	−1.793	−1.794
$\bar{\sigma}_y$ (0.5a, 0.5b, 0.4^+h)	4	−0.8704	−0.8866	−0.8896	−0.8866	−0.8897	−0.8870	−0.8900
	10	−0.8988	−0.9029	−0.9036	−0.9028	−0.9035	−0.9033	−0.9040
	100	−0.9068	−0.9064	−0.9064	−0.9064	−0.9064	−0.9068	−0.9068
$\bar{\sigma}_y$ (0.5a, 0.5b, −0.5h)	4	1.281	−1.000	−1.240	−0.0910	−0.1151	−1.852	−2.089
	10	−0.0753	−0.0902	−0.0956	−0.0802	−0.0856	−0.1443	−0.1497
	100	−0.1333	−0.0894	−0.0895	−0.0792	−0.0792	−0.1371	−0.1372
$\bar{\phi}$ (0.5a, 0.5b, 0.5h)	4	0.1645	–	–	0.0889	0.0530	0.8954	0.8700
	10	0.7564	–	–	−0.0922	−0.1008	0.9938	0.9875
	100	0.9548	–	–	−0.1375	−0.1376	1.017	1.017
$\bar{\tau}_{zx}$ (0, 0.5b, −0.3h)	4	−0.2451	−0.1962	−0.2135	−0.1958	−0.2131	−0.1937	−0.2108
	10	−0.2468	−0.2384	−0.2423	−0.2386	−0.2426	−0.2354	−0.2393
	100	−0.2458	−0.2487	−0.2487	−0.2490	−0.2491	−0.2455	−0.2455

Thus the first and second rows of matrices X^{mn}, $\bar{E}^{mn}$, R^{mn}, $\bar{P}^{mn}$ are the same as in FSDT and the non-zero elements in the third to fifth rows of these matrices are given by

$$X^{mn}_{31} = \bar{m}^3 B_{11} + \bar{m}\bar{n}(2B_{66} + B_{12}), \quad X^{mn}_{32} = \bar{m}^2\bar{n}(B_{12} + 2B_{66}) + \bar{n}^3 B_{22},$$

$$X^{mn}_{34} = \bar{m}^3 D_{11} + \bar{m}\bar{n}^2(2D_{66} + D_{12}), \quad X^{mn}_{35} = \bar{m}^2\bar{n}(D_{12} + 2D_{66}) + \bar{n}^3 D_{22},$$

$$X^{mn}_{43} = \bar{m}, \quad X^{mn}_{44} = 1, \quad X^{mn}_{53} = \bar{n}, \quad X^{mn}_{55} = 1,$$

$$\bar{E}^{mn}_{3,\,2k-2+i} = \left(\bar{m}^2 e^{(k)}_{31} + \bar{n}^2 e^{(k)}_{32}\right)\tilde{\gamma}_{ik}, \quad \bar{P}^{mn}_3 = \left[-p_z + \bar{m}m_x + \bar{n}m_y + \bar{m}^2\left(M^e_1 + M^t_x\right) + \bar{n}^2\left(M^e_2 + M^t_y\right)\right]_{mn}.$$

4. Results and discussion

Results are presented for simply supported hybrid square plate made of 8-layered cross-ply graphite-epoxy laminate $[0^\circ/90^\circ/0^\circ/0^\circ]_s$ with PZT layers bonded to its faces. The orientation is given relative to x-direction. The top PZT layer acts as a sensor and the bottom one as an actuator. All plies of the elastic substrate laminate have equal thickness. The thickness of the sensor layer is taken as $h/10$ and the thickness of the actuator layer has been varied. The properties of graphite-epoxy composite are selected as (see Xu et al., 1995; Kapuria et al., 1999): (E_L, E_T, G_{LT}, G_{TT}) = (181, 10.3, 7.17, 2.87) GPa, $d_{ij} = 0$, $p_3 = 0$, (α_L, α_T) = (0.02, 22.5) × 10^{-6} K^{-1}, (ν_{LT}, ν_{TT}) = (0.28, 0.33),(η_{LL}, η_{TT}) = (30.96, 26.53) × 10^{-12} F/m, (k_L, k_T) = (36.42, 0.96) W m^{-1} K^{-1}, where L and T denote directions parallel and transverse to the fibres, ν_{LT} is Poisson's ratio for strain in the T direction under uniaxial normal stress in the L direction,

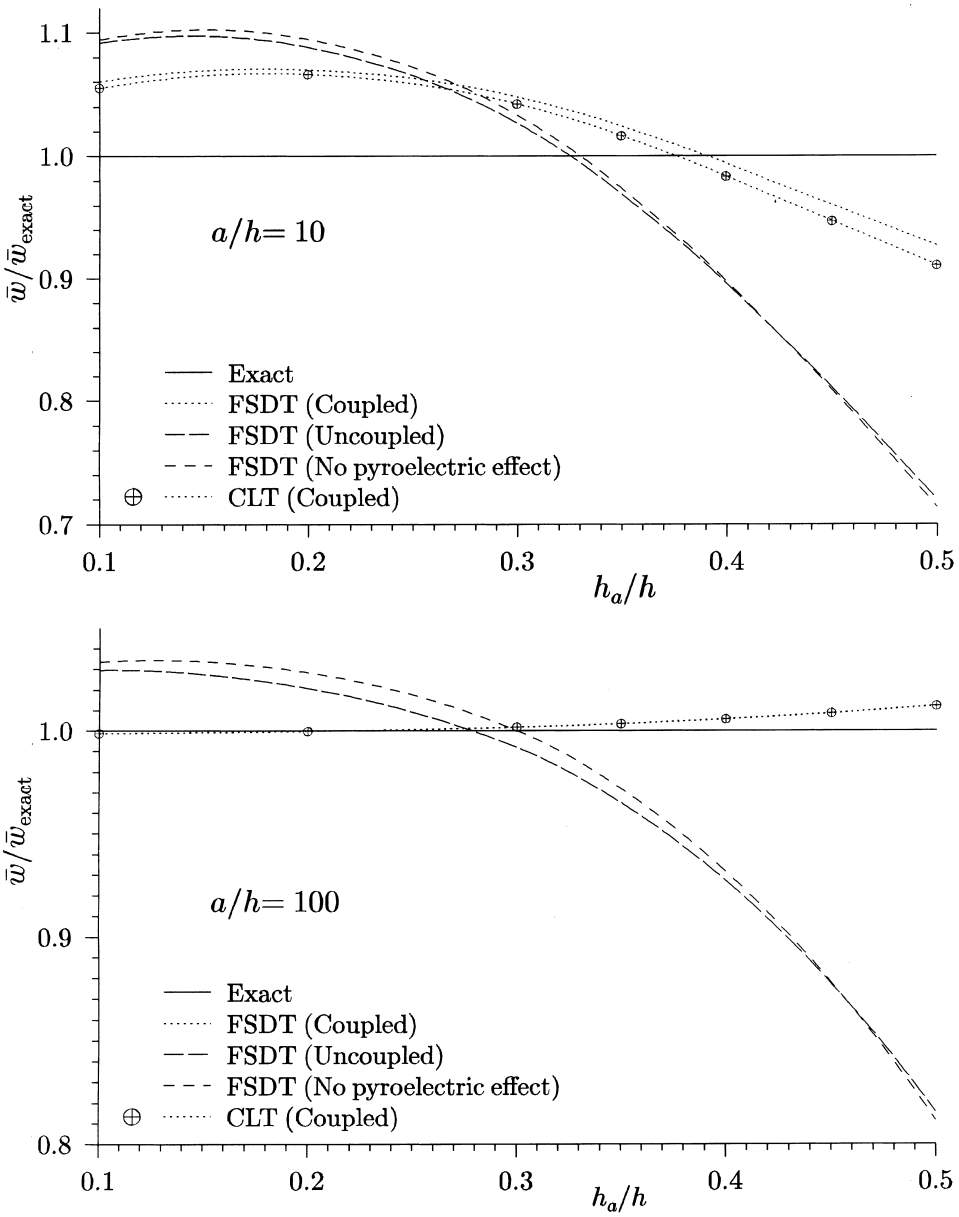

Fig. 1. Effect of h_a/h on $\bar{w}$ (0.5a, 0.5b, 0) for thermal load.

and k_L, k_T are the thermal conductivity coefficients. The properties of PZT are taken as (see Xu et al., 1995, Kapuria et al., 1999): $(E_1, E_2, E_3, G_{12}, G_{23}, G_{31}) = (61.0, 61.0, 53.2, 22.6, 21.1, 21.1)$ GPa, $(\nu_{12}, \nu_{13}, \nu_{23}) = (0.35, 0.38, 0.38)$, $(\alpha_1, \alpha_2, \alpha_3) = (1.5, 1.5, 2.0) \times 10^{-6}$ K^{-1}, $(\eta_{11}, \eta_{22}, \eta_{33}) = (1.53, 1.53, 1.50) \times 10^{-8}$ F/m, $p_3 = 0.0007$ C m^{-2} K^{-1}, $k_1 = k_2 = k_3 = 1.8$ W m^{-1} K^{-1}, $(d_{31}, d_{32}, d_{33}, d_{15}, d_{24}) = (-171, -171, 374, 584, 584) \times 10^{-12}$ m/V.

Following thermal and electrical loads are considered:

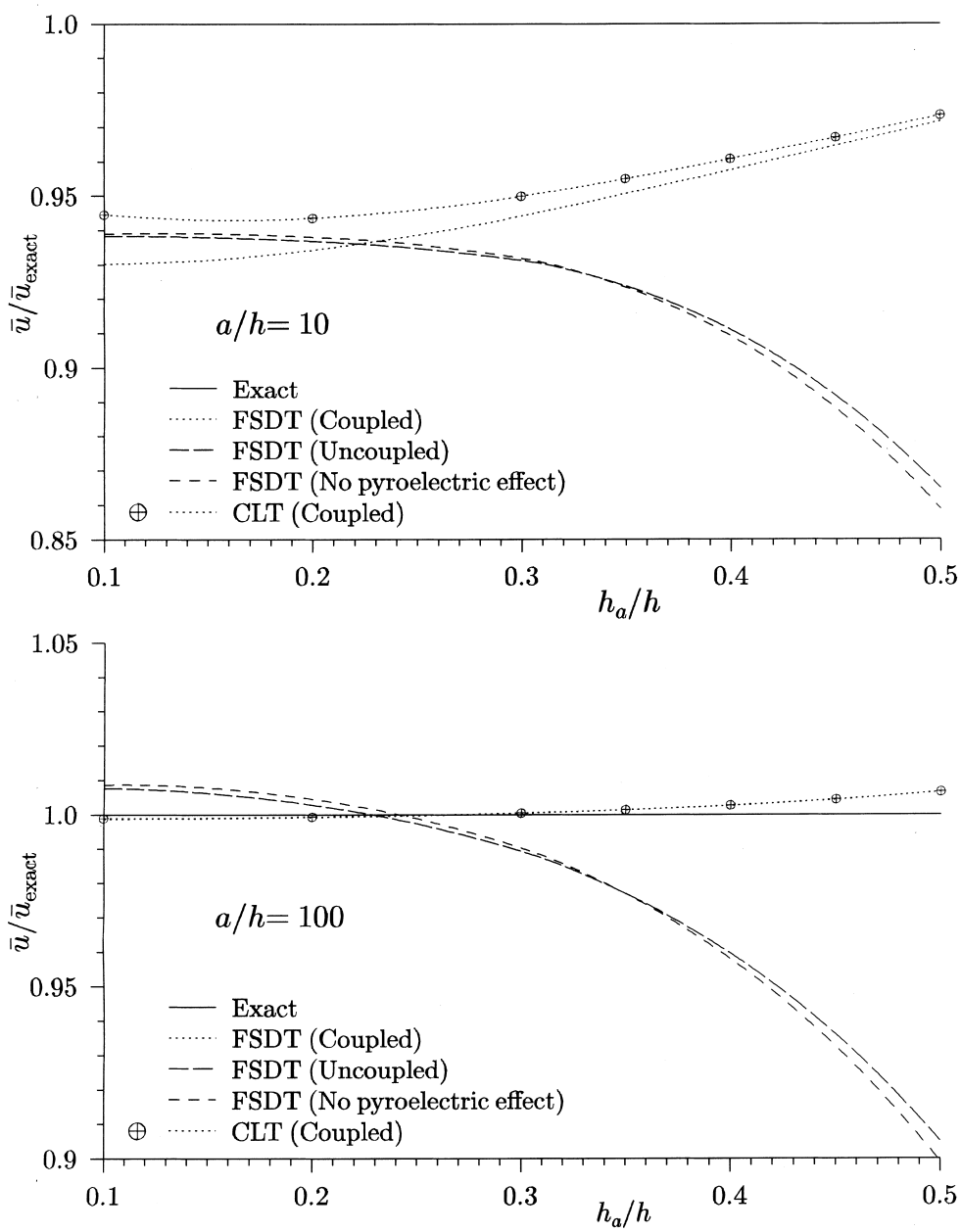

Fig. 2. Effect of h_a/h on $\bar{u}$ (0, 0.5b, −0.5h) for thermal load.

1. a sinusoidal temperature rise at the bottom surface, $T_1 = T_0 \sin(\pi x/a) \sin(\pi y/b)$;
2. an actuating potential applied at the bottom surface, $\phi_1 = \phi_0 \sin(\pi x/a) \sin(\pi y/b)$.

The top surface of the sensor is kept at charge-free condition ($D_2 = 0$) and the interface of the actuator and the substrate is grounded ($\phi_3 = 0$). The results for these loads are nondimensionalised as follows with $S = a/h$. $d_T = 374 \times 10^{-12}$ C N^{-1}:

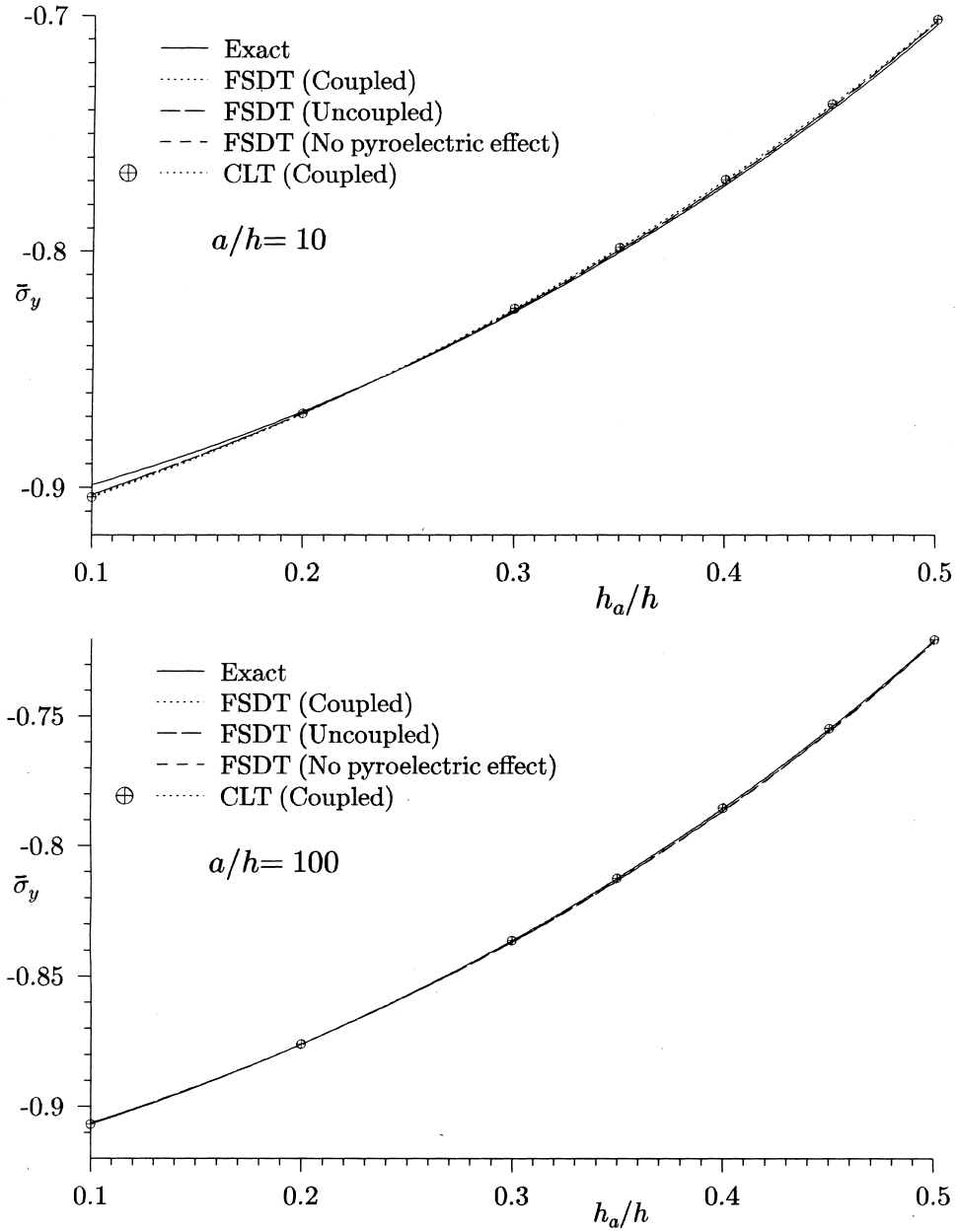

Fig. 3. Effect of h_a/h on $\bar{\sigma}_y$ $(0.5a, 0.5b, -0.5h + h_a^-)$ in the substrate for thermal load.

1. $(\bar{u}, \bar{w}) = 100(u, w/S)/\alpha_T S h T_0$, $(\bar{\sigma}_y, \bar{\tau}_{zx}) = (\sigma_y, \tau_{zx}/S)/\alpha_T E_T T_0$, $\bar{\phi} = 1000\phi d_T/\alpha_T h T_0$;
2. $(\tilde{u}, \tilde{w}) = (u, w/S)/S d_T \phi_0$, $(\bar{\sigma}_x, \bar{\tau}_{yz}) = (\sigma_x, S\tau_{yz})h/E_T d_T \phi_0$.

The uncoupled 2D theories (see e.g. Jonnalagadda et al., 1994), the present coupled 2D theories including the coupling due to direct piezoelectric and pyroelectric effects and the present coupled 2D

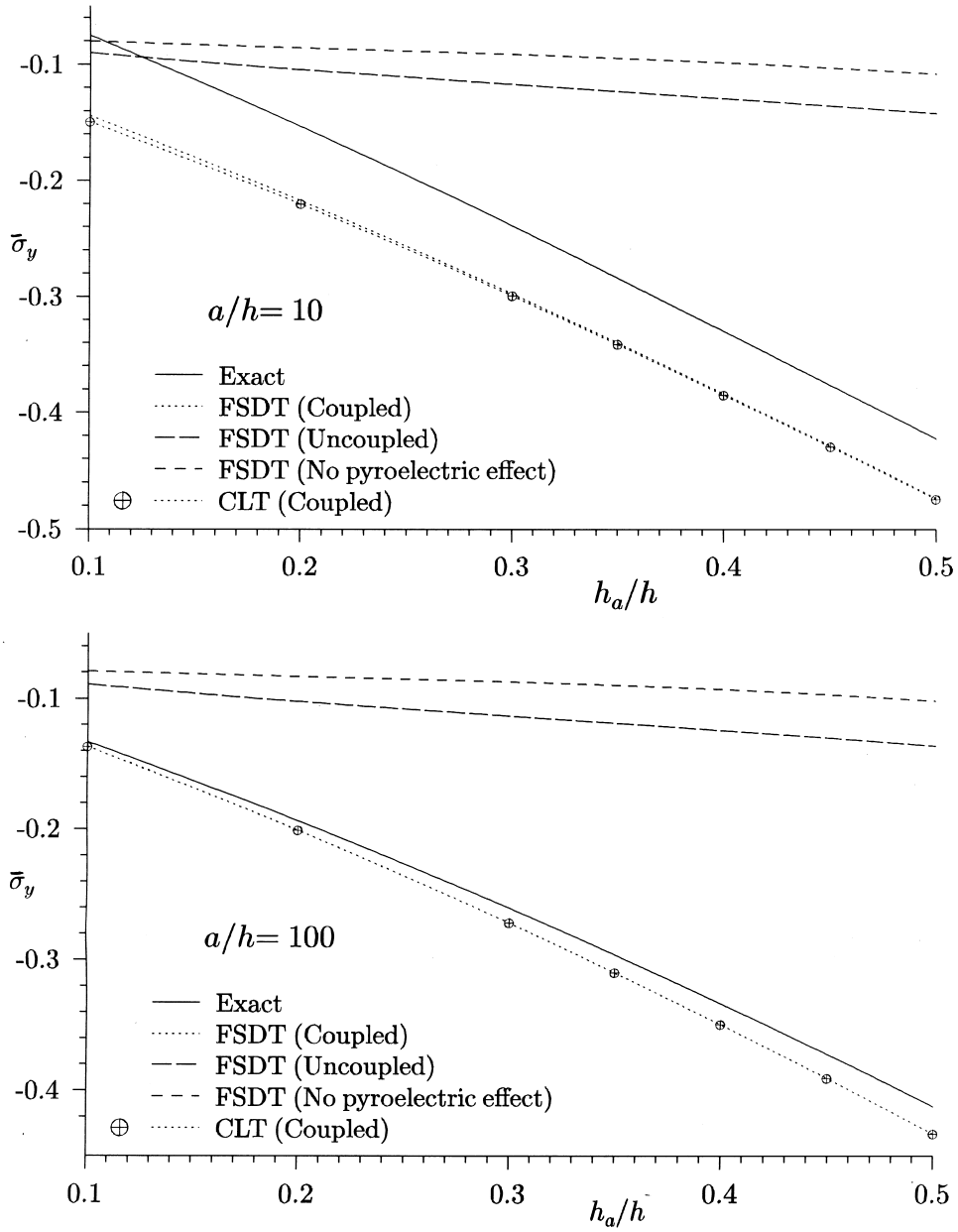

Fig. 4. Effect of h_a/h on $\bar{\sigma}_y$ $(0.5a, 0.5b, -0.5h)$ in the actuator for thermal load.

theories excluding the pyroelectric effect are assessed by comparison with the exact 3D solution presented by Xu et al. (1995) and Kapuria et al. (1999). The results for hybrid plates with actuating layer of thickness $h/10$ subjected to thermal load of case 1 are compared in Table 1. The deflection $\bar{w}$, inplane displacement $\bar{u}$, predominant inplane normal stress $\bar{\sigma}y$ in the substrate and the actuator, predominant transverse shear stress $\bar{\tau}_{zx}$ and induced potential $\bar{\phi}$ are tabulated for three values of S, viz;

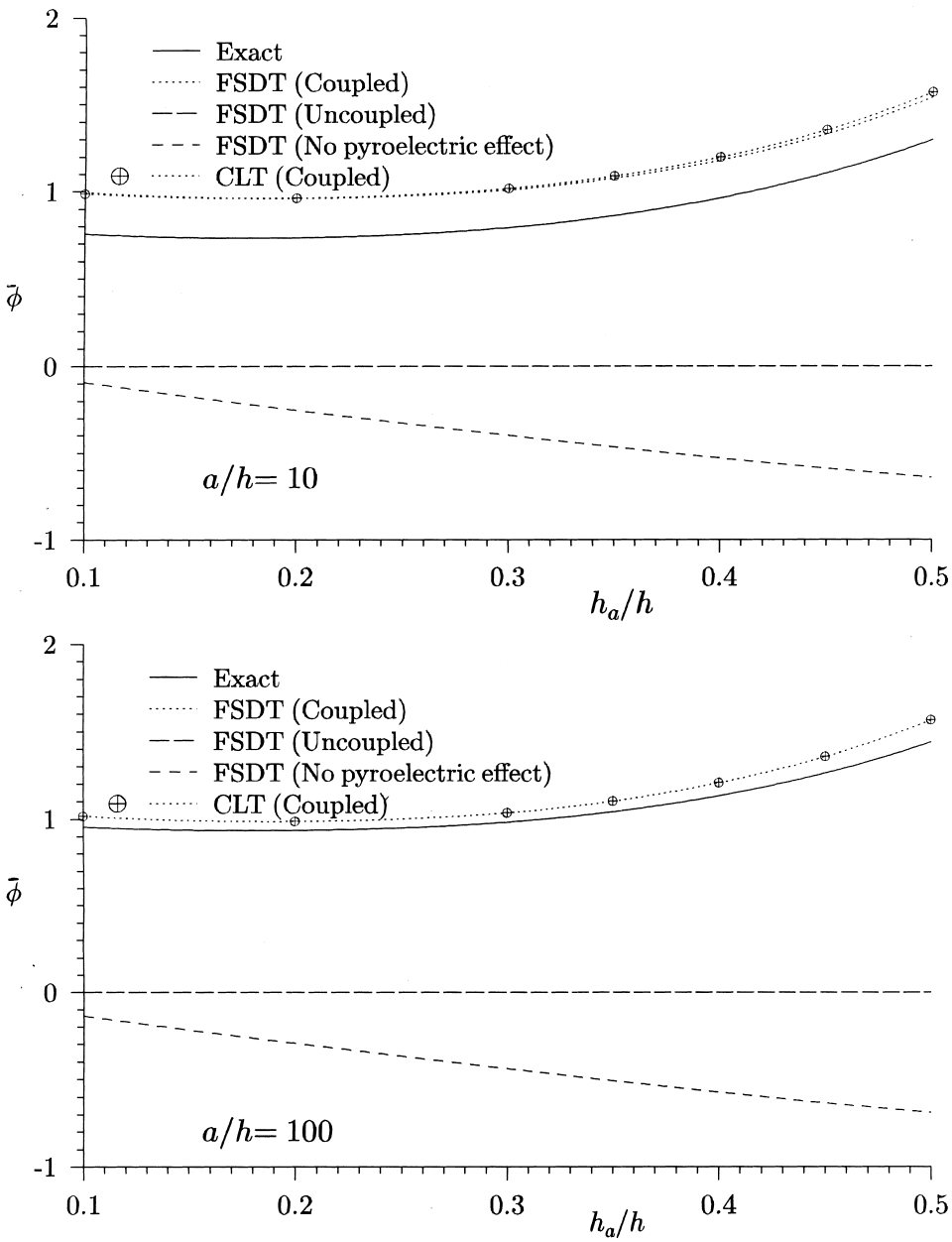

Fig. 5. Effect of h_a/h on sensory potential $\bar{\phi}$ (0.5a, 0.5b, 0.5h) for thermal load.

4 (thick plate), 10 (moderately thick plate) and 100 (thin plate). It is observed that the inclusion of the coupling effect improves the accuracy of the 2D solutions for all the response entities for thin plates, especially so for the stress $\bar{\sigma}_y$ in the actuator layer which is poorly predicted by the uncoupled theories. The potential $\bar{\phi}$ induced in the sensor layer is not directly predicted by the uncoupled theories, but it is very well predicted by the coupled theories for thin to moderately thick plates. It is observed that all

Table 2
Comparative study of 2D solutions for potential load ($h_a/h = 0.1$)

	S	Exact	Uncoupled		Coupled	
			FSDT	CLT	FSDT	CLT
$\bar{w}$ (0.5a, 0.5b, 0)	4	0.2136	0.1735	0.1865	0.1674	0.1801
	10	0.1876	0.1846	0.1865	0.1781	0.1801
	100	0.1810	0.1865	0.1865	0.1801	0.1801
$\bar{u}$ (0, 0.5b, −0.5h)	4	0.4365	0.3874	0.4083	0.3818	0.4021
	10	0.4068	0.4036	0.4083	0.3976	0.4021
	100	0.4030	0.4082	0.4083	0.4020	0.4021
$\bar{\sigma}_x$ (0.5a, 0.5b, 0.4^+h)	4	−19.94	−18.79	−19.70	−18.59	−19.47
	10	−19.48	−19.50	−19.70	−19.27	−19.47
	100	−19.50	−19.70	−19.70	−19.46	−19.47
$\bar{\sigma}_x$ (0.5a, 0.5b, 0.4^-h)	4	2.521	3.216	3.409	4.040	4.181
	10	3.733	3.366	3.409	4.152	4.185
	100	4.077	3.408	3.409	4.185	4.186
$\bar{\sigma}_x$ (0.5a, 0.5b, −0.4$^-$h)	4	30.67	31.84	31.65	32.15	31.98
	10	31.76	31.69	31.65	32.09	32.05
	100	32.00	31.65	31.65	32.07	32.07
$\bar{\tau}_{yz}$ (0.5a, 0, −0.4h)	4	−6.515	−7.907	−8.038	−7.982	−8.107
	10	−7.770	−8.009	−8.038	−8.079	−8.107
	100	−8.094	−8.038	−8.038	−8.107	−8.107

these 2D theories are inaccurate for thick plate with $S = 4$. There is little difference between the results for $\bar{w}$, $\bar{u}$, $\bar{\sigma}_y$, $\bar{\tau}_{zx}$ obtained by the uncoupled 2D theories and the coupled 2D theories without the pyroelectric term. It is concluded that the pyroelectric term has more significant effect than the direct piezoelectric term in case of thermal load. The results of coupled FSDT solution do not show overall improvement over those of coupled CLT solution, there being marginal deterioration in the results of $\bar{w}$, $\bar{u}$, $\bar{\tau}_{zx}$ and slight improvement in those of $\bar{\sigma}_y$ and $\bar{\phi}$.

The effect of the thickness of the actuator layer on the response entities obtained by various 2D theories for plates with $a/h = 10$ and 100 is compared with the exact 3D solution in Figs. 1–5. It is noticed the inclusion of the direct piezoelectric effect in FSDT does not cause any significant change in the results for $\bar{w}$, $\bar{u}$ and $\bar{\sigma}_y$ in the substrate. Coupling due to pyroelectric term has significant effect on the displacements, particularly for the thicker actuator layers. For thin plates, coupled 2D theories (including both pyroelectric and direct piezoelectric effect) yield significant improvement in the values of $\bar{w}$, $\bar{u}$ for all values of h_a/h. In general, the coupled theories yield better estimates of the displacements for moderately thick plates as well, except for some intermediate range of values of the actuator thickness. The improvement in these results is more pronounced for larger thickness of the actuator layer. Fig. 3 shows that the electrothermomechanical coupling does not have any appreciable effect on the stress $\bar{\sigma}_y$ in the substrate. However, it is observed from Fig. 4 that the stress $\bar{\sigma}_y$ in the actuator is significantly affected by coupling. The 2D coupled theories yield substantial improvement in the values of $\bar{\sigma}_y$ in the actuator for thin plates as well as for moderately thick plates. The coupled FSDT theories predict much better the stress $\bar{\sigma}_y$ in the actuator layer as its thickness increases. It is noticed from Fig. 5 that the coupled theories predict very well the sensory potential induced in the top surface for thin to moderately thick plates. Inclusion of only the direct piezoelectric effect in FSDT is found to worsen the estimate for the stress $\bar{\sigma}_y$ in the actuator and the potential in the sensor.

Results for midsurface deflection $\tilde{w}$, inplane displacement $\tilde{u}$ at the bottom surface, predominant normal stress $\tilde{\sigma}_x$ at the top and bottom of the substrate, $\tilde{\sigma}_x$ at the top of the actuator and predominant

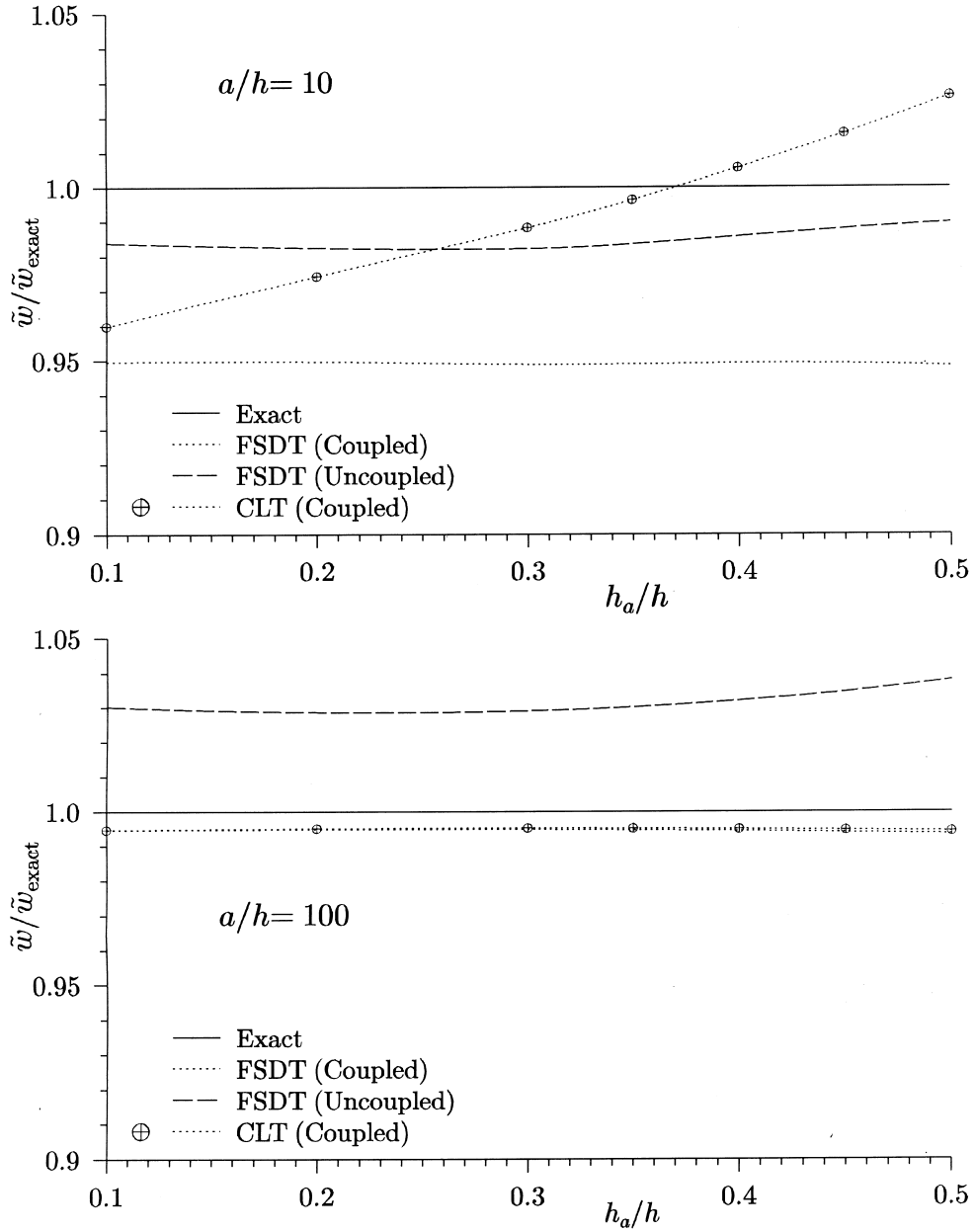

Fig. 6. Effect of h_a/h on $\tilde{w}$ (0.5a, 0.5b, 0) for potential load.

transverse shear stress $\tilde{\tau}_{yz}$ at the actuator-substrate interface in hybrid plates under sinusoidal potential load of case 2 are presented in Table 2. In this case the coupling is due to the direct piezoelectric effect only. It is observed that for the thin plates the coupled 2D solutions for all the response entities are much closer to the 3D exact solution. However, for the present case, the results of the coupled 2D solutions for the thicker plates show slight deterioration relative to those for the uncoupled 2D

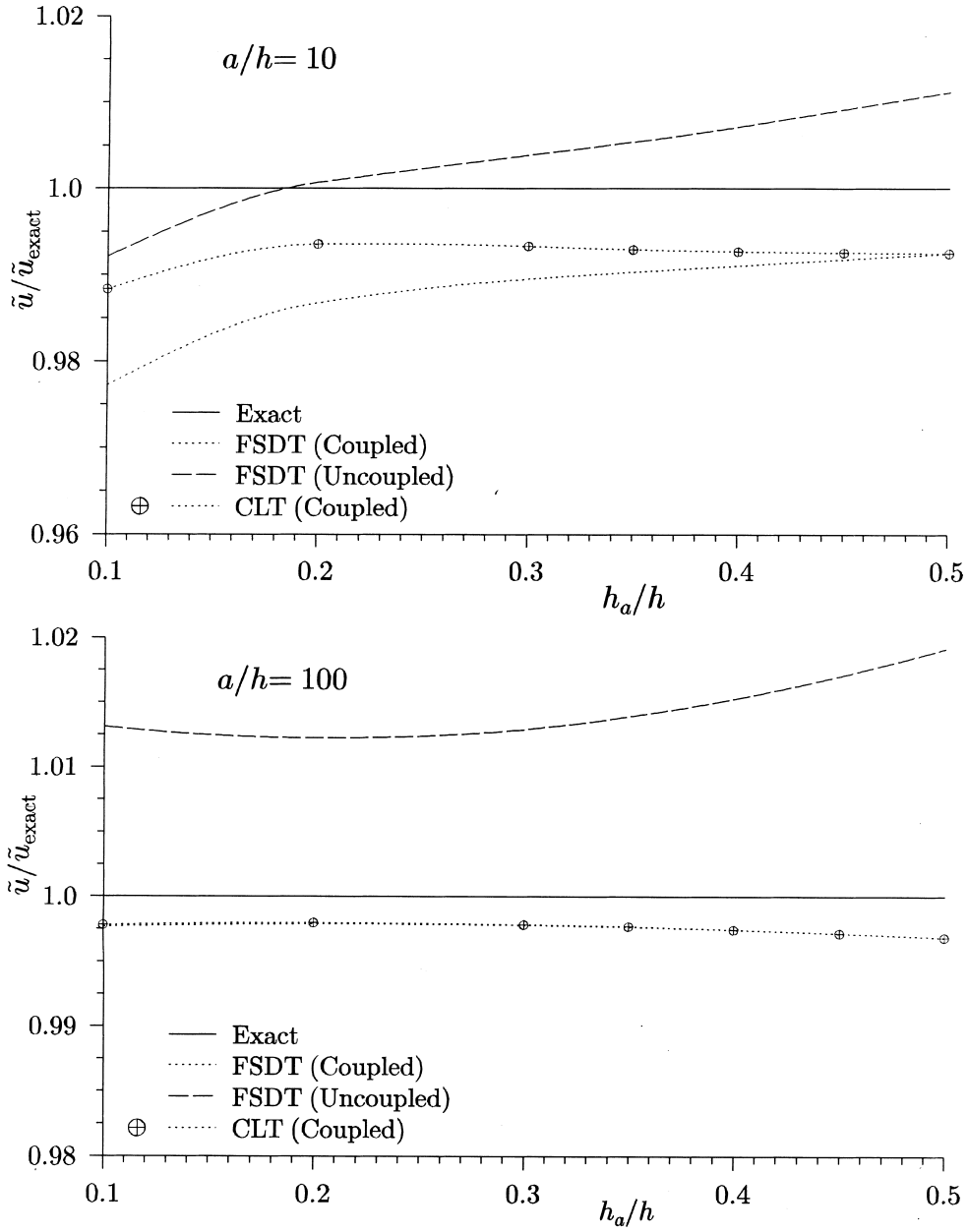

Fig. 7. Effect of h_a/h on $\tilde{u}$ (0, 0.5b, −0.5h) for potential load.

solutions. It is observed the the inclusion of the shear deformation effect in the 2D theory does not improve the results. The effect of the actuator thickness ratio, h_a/h, on the response for the potential load case is shown in Figs. 6–11. These figures reveal that for thin hybrid plates the coupled 2D theories yield more accurate results than the uncoupled ones for all values of h_a/h. The coupling does not have much effect on the maximum inplane stress $\tilde{\sigma}_x$ in the substrate at the bottom interface (Fig. 8). Fig. 9–

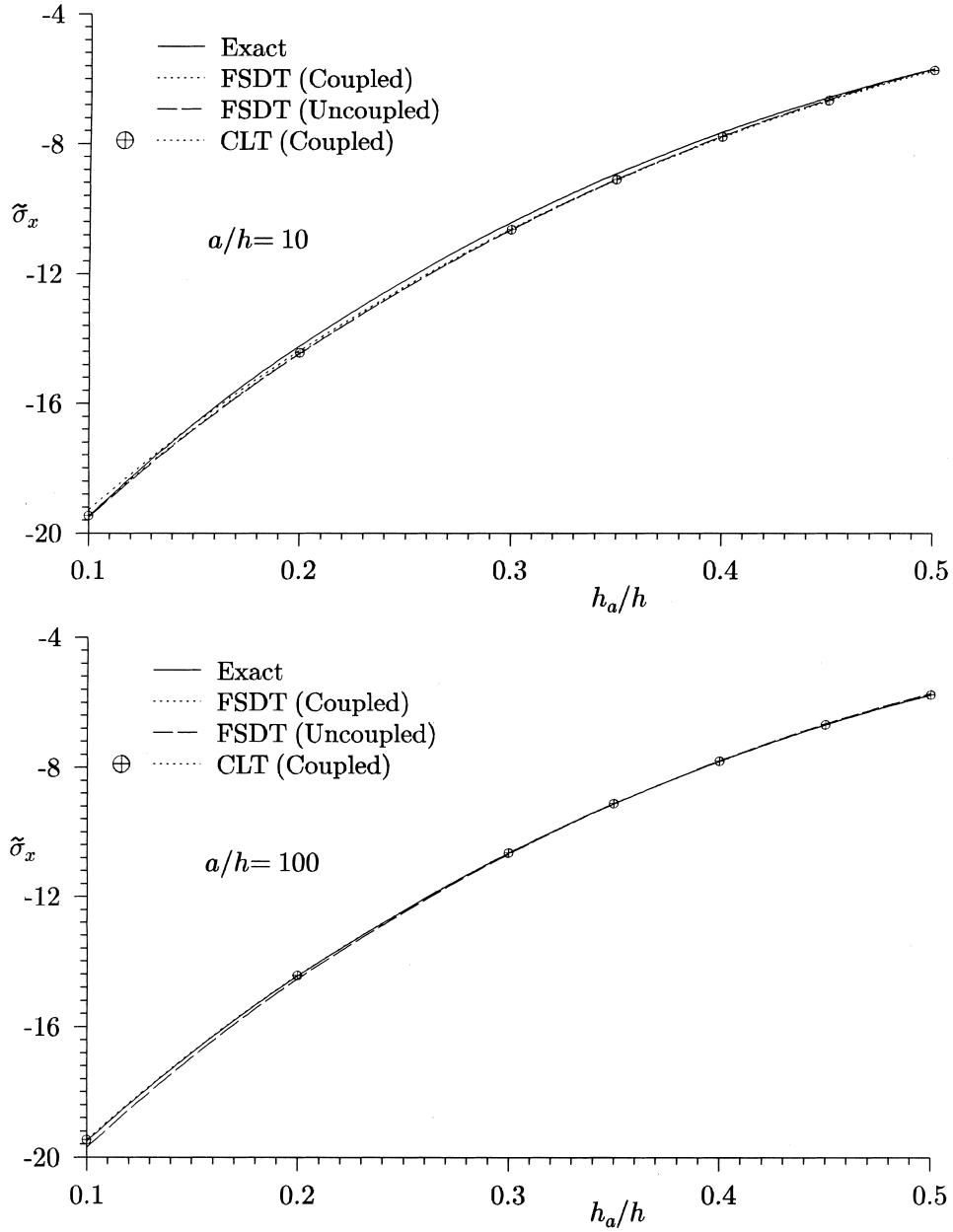

Fig. 8. Effect of h_a/h on $\tilde{\sigma}_x$ $(0.5a, 0.5b, -0.5h + h_a^-)$ at bottom of the substrate for potential load.

11 reveal that the inplane stress $\tilde{\sigma}_x$ at the top interface of the substrate, the inplane stress $\tilde{\sigma}_x$ in the actuator and the shear stress $\tilde{\tau}_{yz}$ at the actuator-substrate interface are predicted more accurately by the coupled 2D theories than the uncoupled ones. The effect of coupling becomes more pronounced as the actuator thickness increases. The stress $\tilde{\sigma}_x$ in the actuator is better estimated by including the coupling effect for thicker plates as well.

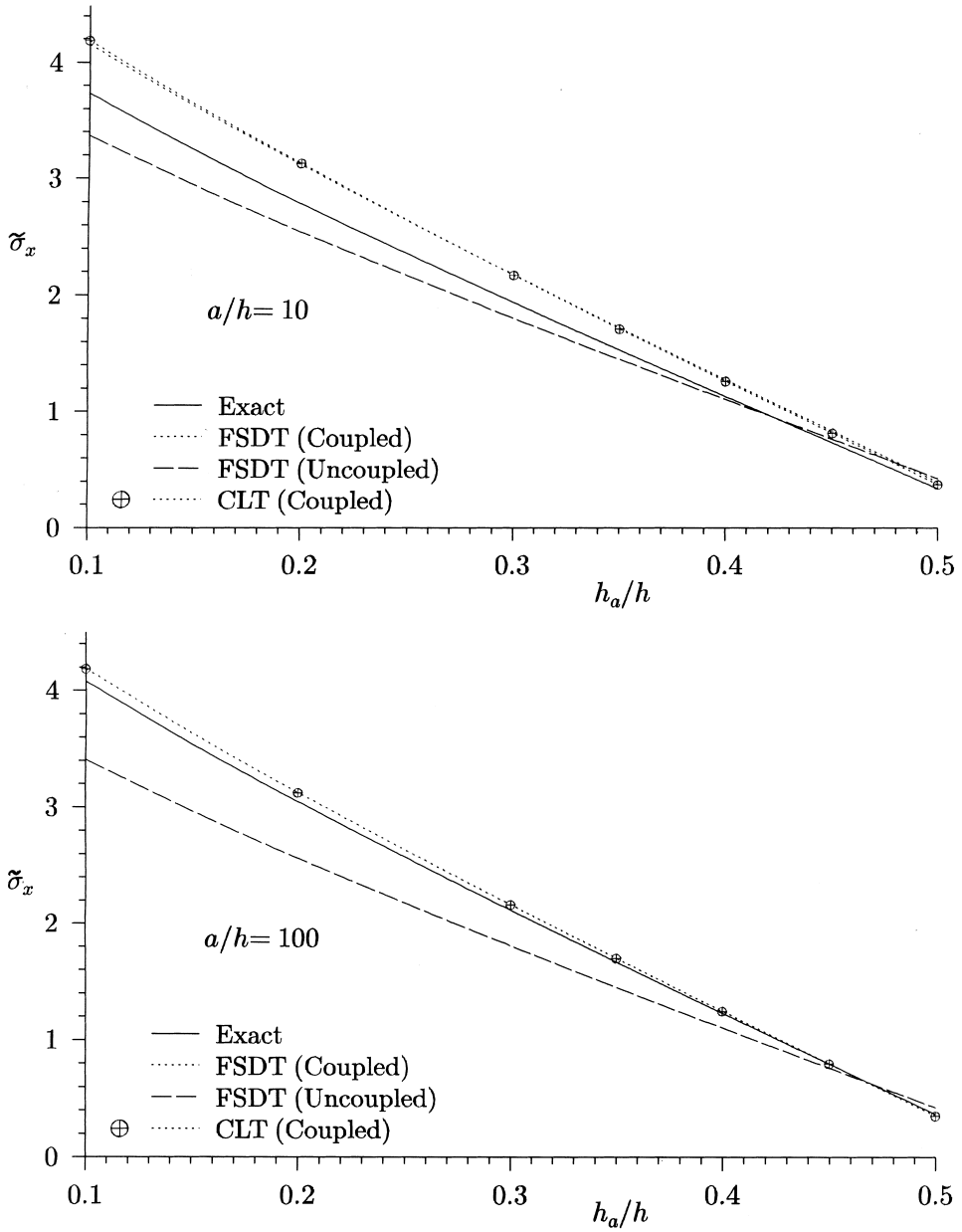

Fig. 9. Effect of h_a/h on $\tilde{\sigma}_x$ $(0.5a, 0.5b, 0.4h^-)$ at top of the substrate for potential load.

5. Conclusions

Coupled CLT and FSDT formulations are presented for simply-supported hybrid rectangular plate without any adhoc assumptions on the through-the-thickness variations of electric potential and temperature. The comparison of these 2D coupled theories with the 2D uncoupled and 3D exact

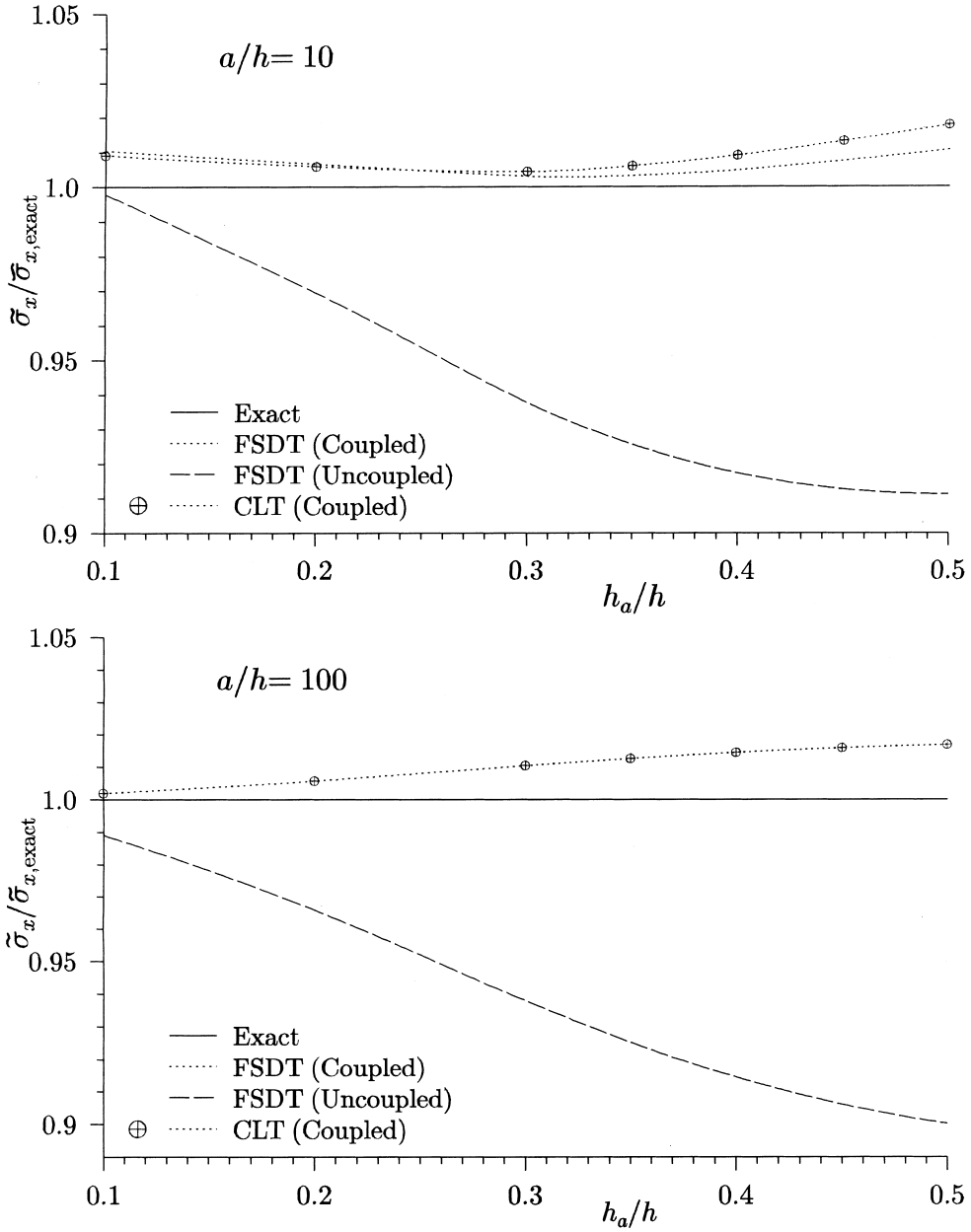

Fig. 10. Effect of h_a/h on $\tilde{\sigma}_x$ $(0.5a, 0.5b, -0.5h)$ in the actuator for potential load.

solutions reveals that the pyroelectric effect is predominant in case of thermal loading, whereas the direct piezoelectric effect is significant in the potential load case. The inclusion of the coupling effect significantly improves the 2D solutions for thermal and potential loads for thin plates. The coupling has significant effect on the displacements, the inplane stress in the actuator and the interlaminar shear stress at the substrate-actuator interface. The effect of the coupling generally increases with the thickness of

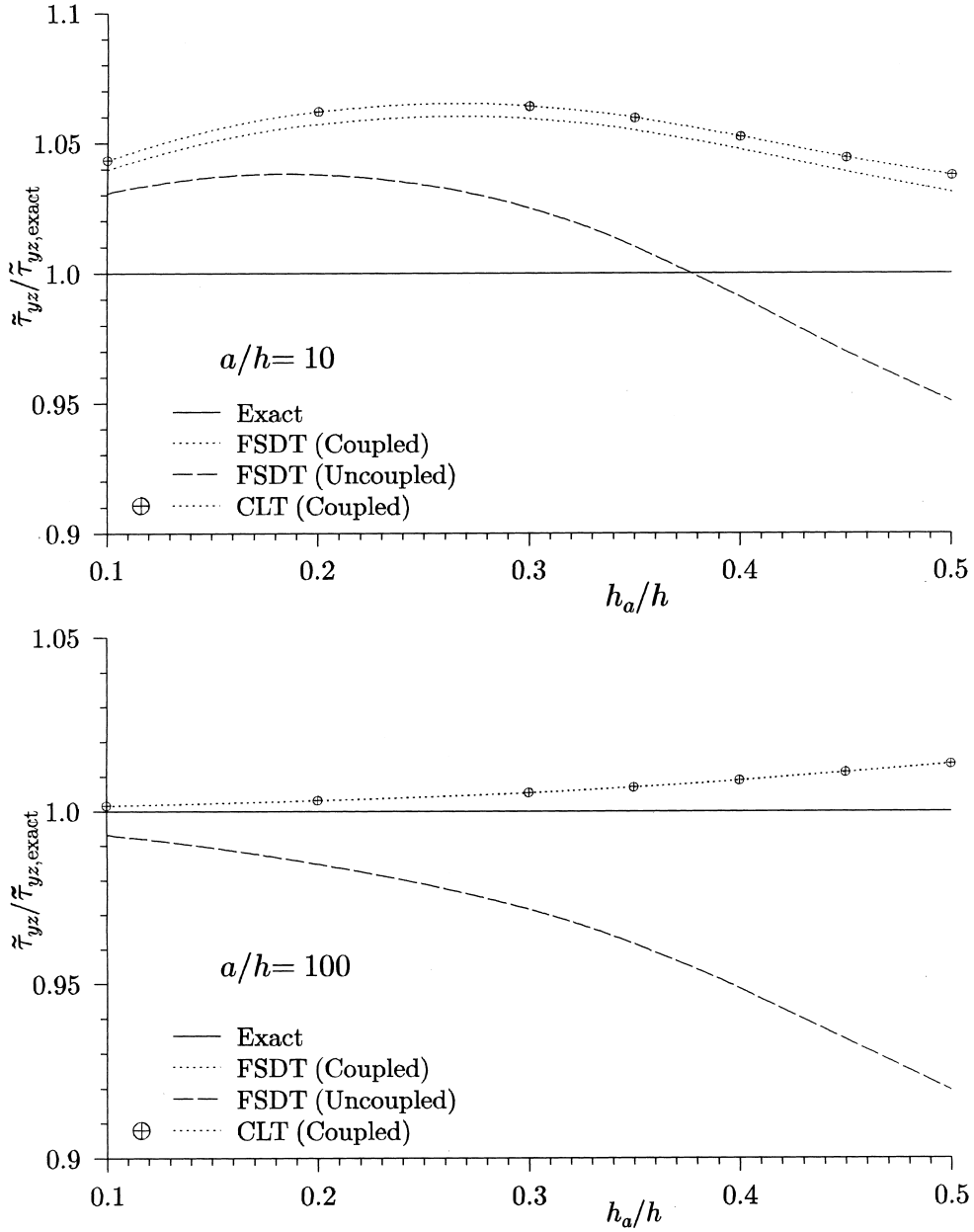

Fig. 11. Effect of h_a/h on $\tilde{\tau}_{yz}$ $(0.5a, 0, -0.4h)$ for potential load.

the actuator layer. The coupling does not have any apprciable effect on the maximum value of the inplane normal stress in the substrate for the two load cases. The coupled theories predict the sensory potential very well for thin to moderately thick plates. The coupled FSDT solution shows marginal improvement in some results and slight deterioration in others. Therefore, there is a need to improve upon the incorporation of the shear deformation effect in a 2D theory.

References

Dube, G.P., Kapuria, S., Dumir, P.C., 1996. Exact piezothermoelastic solution of simply-supported orthotropic flat panel in cylindrical bending. Int. J. Mech. Sci 38, 1161–1177.

Jonnalagadda, K.D., Blandford, G.E., Tauchert, T.R., 1994. Piezothermoelastic composite plate analysis using first-order shear deformation theory. Computers and Structures 51, 79–89.

Kapuria, S., Dube, G.P., Dumir, P.C., 1997. Exact piezothermoelastic solution for simply supported laminated flat panel in cylindrical bending. ZAMM 77, 281–293.

Kapuria, S., Dumir, P.C., Sengupta, S., 1999. Three dimensional solution for shape control of simply supported rectangular plate. J. Thermal Stresses 22, 159–176.

Noda, N., Kimura, S., 1998. Deformation of piezothermoelastic composite plate considering coupling effect. J. Thermal Stresses 21, 359–379.

Ray, M.C., Rao, K.M., Samanta, B., 1992. Exact analysis of coupled electroelastic behavior of a piezoelectric plate under cylindrical bending. Comput. Struct 45, 667–677.

Tang, Y.Y., Noor, A.K., Xu, K., 1996. Assessment of computational models for thermoelectroelastic multilayered plates. Computers and Structures 61, 915–933.

Tauchert, T.R., 1992. Piezothermoelastic behavior of a laminated plate. J. Thermal Stresses 15, 25–37.

Tzou, H.S., Ye, R., 1994. Piezothermoelastic and precision control of piezoelectric systems, theory and finite element analysis. J. Vibration and Accoustics 116, 489–495.

Xu, K., Noor, A.K., Tang, Y.Y., 1995. Three-dimensional solutions for coupled thermoelectroelastic response of multilayered plates. Comput. Methods Appl. Mech. Engng 126, 355–371.